ACS APPLIED MATERIALS & INTERFACES
Research Article
www.acsami.org

Polyaniline-Assisted Synthesis of Si@C/RGO as Anode Material for Rechargeable Lithium-Ion Batteries

Ning Lin, Jianbin Zhou, Liangbiao Wang, Yongchun Zhu,* and Yitai Qian*

Department of Chemistry and Hefei National Laboratory for Physical Science at Microscale, University of Science and Technology of China, Hefei, Anhui 230026, P. R. China

Supporting Information

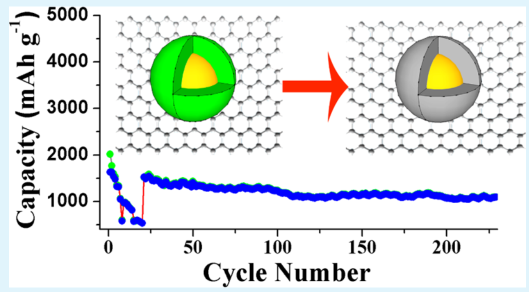

ABSTRACT: A novel approach to fabricate Si@carbon/reduced graphene oxides composite (Si@C/RGO) assisted by polyaniline (PANI) is developed. Here, PANI not only serves as "glue" to combine Si nanoparticles with graphene oxides through electrostatic attraction but also can be pyrolyzed as carbon layer coated on Si particles during subsequent annealing treatment. The assembled composite delivers high reversible capacity of 1121 mAh g^{-1} at a current density of 0.9 A g^{-1} over 230 cycles with improved initial Coulombic efficiency of 81.1%, while the bare Si and Si@carbon only retain specific capacity of 50 and 495 mAh g^{-1} at 0.3 A g^{-1} after 50 cycles, respectively. The enhanced electrochemical performance of Si@C/RGO can be attributed to the dual protection of carbon layer and graphene sheets, which are synergistically capable of overcoming the drawbacks of inner Si particles such as huge volume change and low conductivity and providing protective and conductive matrix to buffer the volume variation, prevent the Si particles from aggregating, enhance the conductivity, and stabilize the solid−electrolyte interface membrane during cycling. Importantly, this method opens a novel, universal graphene coating strategy, which can be extended to other fascinating anode and cathode materials.

KEYWORDS: *polyaniline assistance, Si particles, graphene, dual protection, lithium-ion batteries*

INTRODUCTION

Silicon (Si) has been considered as the promising anode material for lithium-ion battery due to its highest theoretical gravimetric capacity (3579 mAh g^{-1}), low discharging potential (<0.5 V vs Li/Li$^+$), relatively abundant resource on the earth, and eco-friendly properties.[1,2] However, practical application of Si-based anodes is seriously restricted by the low intrinsic electric conductivity and huge volume change (over 270%) during lithium ion insertion/extraction process, which directly results in the pulverization of anode structure, unstable growth of solid−electrolyte interface (SEI), and thus rapid capacity degradation.[3,4]

Graphene, as one kind of two-dimensional (2D) materials with excellent mechanical properties and conductive network, has been extensively studied to combine with Si materials.[5,6] These unique advantages enable the graphene-based composite to accommodate the volume change and improve the conductivity.[7,8] Recently, several efforts have been made to fabricate Si and graphene composites that exhibit enhanced electrochemical performance. For example, Cao et al. fabricated Si/graphene composite through self-assembly of NH_2-terminated Si nanowires and graphene oxides, which exhibits high capacity retention of 1335 mAh g^{-1} after 80 cycles at 0.2 A g^{-1}.[9] Guo et al. developed a method to endow Si particles with positive charge by enwrapping poly(diallydimethylammonium chloride) and then self-assembled with graphene oxide (GO); the synthesized composite shows a reversible capacity of 1205 mAh g^{-1} over 150 cycles at 0.1 A g^{-1}.[10]

Yet, open channels, constructed by the simple combination of Si nanoparticles with graphene sheets, allow the direct contact of Si with the electrolyte, which results in side reaction and formation of unstable SEI membrane.[11] To address these issues, the way to coat carbon on Si has been proved to be an efficient method to avoid the direct contact of Si and electrolyte, because carbon layer plays a vital role in stabilizing SEI films and suppressing the aggregation of Si during repeated lithiation/delithiation process.[12,13]

In this study, to make full use of the merits of graphene and carbon additives, we developed a novel strategy to fabricate Si@carbon/reduced graphene oxides composite (Si@C/RGO) by covering Si particles with carbon and graphene assisted by polyaniline (PANI), as shown in Scheme 1. First, PANI was coated on as-synthesized Si particles through oxidative polymerization in situ, which distributed positive charge on the surface of Si particles. Then, the positively charged intermediate was assembled with negatively charged GOs through electrostatic interaction, where PANI served as "glue" to bind Si with GO sheets tightly. Finally, heat-treatment was conducted to reduce GO as RGO and pyrolyze deposited PANI

Received: September 17, 2014
Accepted: December 11, 2014
Published: December 11, 2014

Scheme 1. Schematic Picture of the Synthesis Route of Si@C/RGO[a]

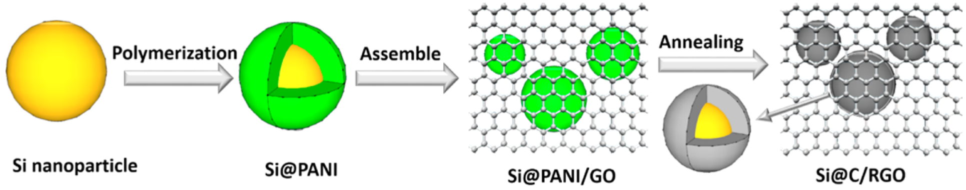

[a]The images of the raw product and intermediate products are only schematic illustrations that do not exactly reflect the real structures.

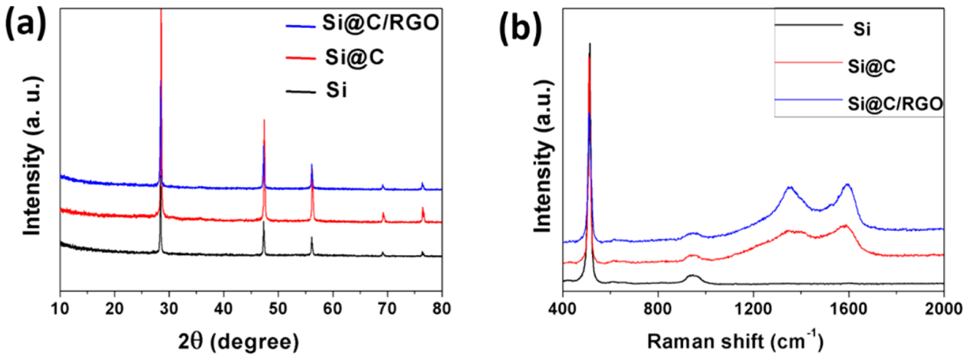

Figure 1. (a) X-ray diffraction patterns and (b) Raman spectra of as-synthesized Si, Si@C, and Si@C/RGO.

as carbon layer on Si surface, which makes the Si particles in the composite get dual protection. As an anode material for rechargeable lithium-ion batteries, the Si@C/RGO composite delivers a reversible capacity of 1121 mAh g^{-1} at 0.9 A g^{-1} after 230 cycles, with improved initial Coulombic efficiency of 81.1%, while the bare Si and Si@C retain a negligible capacity of 50 and 495 mAh g^{-1} after 50 cycles, with initial Coulombic efficiency of 56.2% and 72.3%, respectively. The enhanced performance of Si@C/RGO could be attributed to this unique structure, which is beneficial for buffering the volume variation, accelerating electron transfer, suppressing Si particles aggregating, and stabilizing the SEI films.

■ EXPERIMENTAL SECTION

All the reagents used here are of analytical grade without further purification.

Preparation of Si. Silicon was prepared through a typical magnesiothermic reduction of commercial silica, as shown in eq 1.[14] Magnesium (Mg) and silica (with a molar ration of 2 to 1) were mixed uniformly and maintained temperature at 650 °C for 10 h in stainless steel autoclave. The product was collected and washed with diluted hydrochloric acid, distilled water, and absolute ethanol several times. The residual silicon oxides were removed by soaking the product in ethanol-based hydrofluoric acid for 3 h.

$$2Mg + SiO_2 \leftrightarrow 2MgO + Si \quad (1)$$

Fabrication of Si@C/RGO. The Si@C/RGO composite was fabricated by three steps, as shown in Scheme 1. First, Si@PANI composite was obtained by oxidization polymerization in situ.[15] In a typical experiment, 70 mg of Si and 0.15 g of aniline were added into 15 mL of distilled water. And then the pH of the suspension was adjusted to 1 by adding a few drops of concentrated hydrochloric acid (denoted as suspension A). After ultrasonication for 0.5 h, ammonium persulfate solution (0.090 g in 5 mL of water) was added to suspension A as oxidant to start the polymerization. Then the mixed suspension was stirred overnight in ice bath. Upon polymerization, the color of suspension changed from brown to dark green, indicating the formation of the PANI coating on Si, as shown in Supporting Information, Figure S1. Second, the obtained Si@PANI was redispersed in 100 mL of distilled water through ultrasonic dispersion. Then 35 mL of 0.8 mg mL^{-1} graphene oxide (GO) suspension was added. The GO suspension was prepared with modified Hummer's method, details in Supporting Information. After the suspension was vigorously stirred for 1 h, the resultant Si@PANI/GO was collected by centrifuging at 3000 rpm. Finally, Si@C/RGO was obtained by annealing treatment of the preassembled composite at 600 °C for 2 h under argon atmosphere. On the basis of the yield value, the percentage of Si in the composite was about 70%, calculated by the average yield value of a few times of experiments. As a contrast sample, Si@C composite was fabricated following the similar procedure without adding GO.

Structural Characterization. The morphology and structure of these samples in this work were characterized by X-ray diffraction (Philips X'Pert Super diffractometer with Cu Kα radiation (λ = 1.541 78 Å)), Raman spectrometer (Lab-RAM HR UV/vis/NIR), scanning electron microscopy (SEM) (JSM-6700F), Fourier transformed infrared spectroscopy (FTIR, Hyperion 3000), and transmission electron microscopy (TEM) (JEOL-2010).

Electrochemical Measurements. Half-cell tests were conducted using two electrode coin-type cells (CR2016) with pure Li metal foil as counter and reference electrode. For preparing working electrode, a slurry mixture of as-prepared active materials, super P, and carboxymethylcellulose sodium (CMC-Na) at a weight ratio of 70:25:5, was coated on copper foil (99.9%). A solution of 1 M $LiPF_6$ in ethylene carbonate (EC) and diethyl carbonate (DEC) (1:1 in volume ratio) served as electrolyte. The cells were assembled in an argon-filled glovebox. Note that we adopted a copper foil with diameter size of 12 mm and pasted the slurry with the thickness of 150 μm and the mass of 2.0 mg approximately. Galvanostatic charge/discharge measurements were carried out on a LAND-CT2001A instrument with a fixed voltage range of 0.01−1.5 V (vs Li/Li^+). Unless otherwise noted, charge/discharge rate and specific capacity were calculated based on the total mass of active materials. Cyclic voltammetry (CV) was performed on electrochemical workstation (CHI660D), with a scanning rate of 0.2 mV s^{-1} at room temperature. Electrochemical impedance spectroscopy (EIS) was also measured with an electrochemical workstation (CHI660D) by applying an alternating current (AC) voltage of 5 mV in the frequency range from 100 kHz to 0.1 Hz.

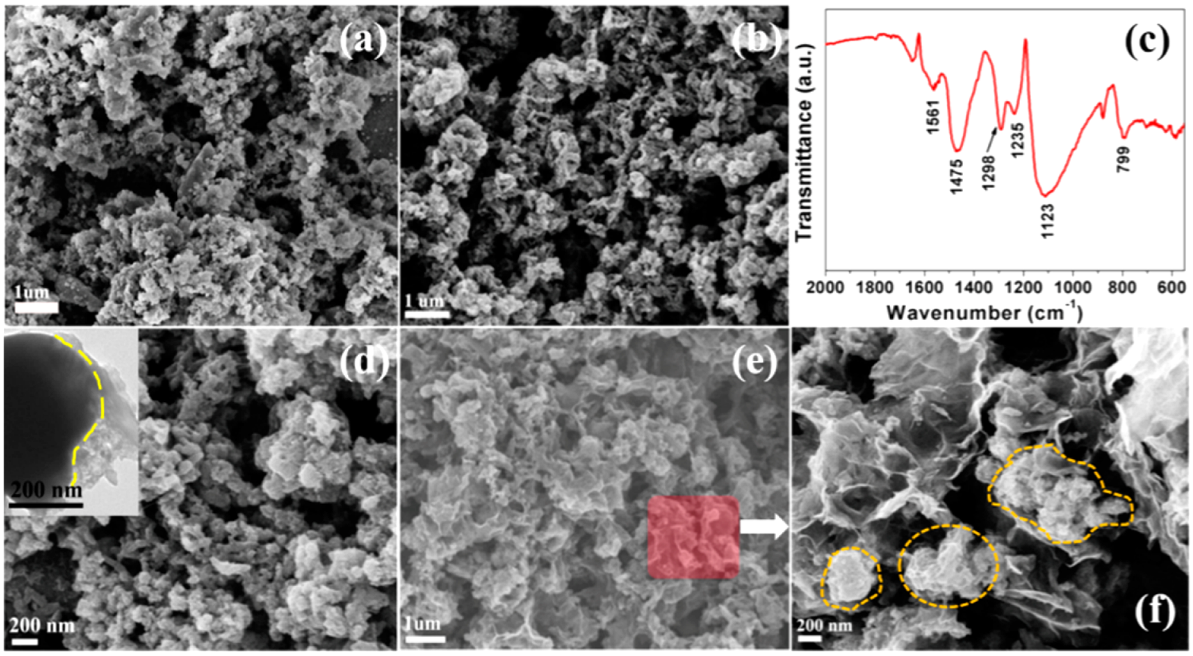

Figure 2. Scanning electron microscopy (SEM) images of (a) Si nanoparticles, (b) Si@PANI, (d) Si@C, (e) Si@C/RGO, (f) enlarged image of Si@C/RGO. (c) FTIR spectrum for Si@PANI composite.

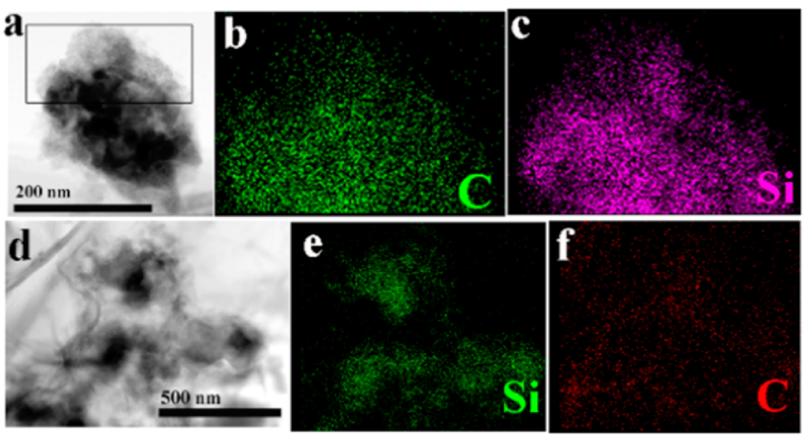

Figure 3. Transmission electron microscopy (TEM) and the corresponding elemental mapping pictures of (a–c) Si@C and (d–f) Si@C/RGO composite, respectively.

RESULTS AND DISCUSSION

Figure 1a shows the X-ray diffraction patterns of bare Si, Si@C, and Si@C/RGO. In all three samples, the major diffraction peaks of 28.5, 47.5, and 56.3° can be indexed to lattice plane of (111), (220), and (311) of well-crystallized silicon, respectively.[16,17] The typical Raman spectrum of bare Si, Si@C, and Si@C/RGO are exhibited in Figure 1b. The strong peak at ~515 cm^{-1}, representing silicon, as well as Raman secondary diffraction peaks, are clearly present in Si, Si@C, and Si@C/RGO samples.[18] And these peaks at 1340 and 1584 cm^{-1} of Si@C and Si@C/RGO are named as D band and G band of graphite, respectively. The D band (~1340 cm^{-1}) is associated with the vibration of carbon atoms with dangling bonds in-plane terminations of disordered graphite. The G band (~1584 cm^{-1}) is assigned to an E_{2g} vibration mode of graphite and is related to the vibration of sp^2-bonded carbon atoms in a 2D hexagonal lattice.[19] It is reasonable to conclude that heating treatment has made the PANI pyrolyzed as carbon layer.[20] Compared with Si@C, the intensity ratio of D and G band of Si@C/RGO is significantly improved, which mainly results from RGO.

The morphology of the prepared samples is first elucidated by scanning electron microscope (SEM). Figure 2a exhibits the SEM image of as-prepared Si, which are irregular nanoparticles with a size of ~100 nm. The SEM image of Si@PANI composite is presented in Figure 2b. Si nanoparticles are covered by shaggy PANI, and no independent Si particles can be found. It is reasonable to suppose that Si nanoparticles, aniline, and ammonium persulfate were evenly dispersed in the aqueous suspension, and the negatively charged Si surface was utilized as substrate for the growth of PANI. After polymerization, the Si surface was completely covered with positive charge, which offers a bridge to coalesce negatively charged GO with Si through electrostatic interaction.[17,21] Figure 2c shows the FTIR spectrum of Si@PANI composite, which contains a group of typical bands of PANI, namely, C=C stretching of the quinonoid ring and benzenoid ring at 1561 and 1475 cm^{-1},

dx.doi.org/10.1021/am506404b | ACS Appl. Mater. Interfaces 2015, 7, 409−414

respectively, C−N stretching of secondary aromatic amines at 1298 cm^{-1}, and C−H bending of the benzenoid ring and the quinonoid ring at 1235 and 1123 cm^{-1}, respectively.[21,22] And the peak located at 799 cm^{-1} represents the symmetrical stretching vibration of Si−O, because the Si atoms on the particle surface were oxidized in the air.

Figure 2d shows the SEM image of Si@C. What we can observe only is the rough surface, which keeps similar to the morphology of initial PANI coated on Si particles. And the corresponding TEM image is presented in the inset; a clear carbon layer coated on Si particles is detected. Figure 2e shows the SEM picture of Si@C/RGO, compared with Si@C, the rough surface is replaced by smooth and undulating surface because a large amount of RGO sheets enwrap the Si@C cores completely through aforementioned procedure. Figure 2f shows the magnified SEM image of Si@C/RGO; clearly, the Si nanoparticles with irregular structure are encapsulated into some pieces of RGO sheets.

In addition, the Si@C and Si@C/RGO composites are analyzed by TEM and corresponding elemental mapping with regard to the distribution of Si and C elements, as shown in Figure 3. Figure 3a−c exhibits that the Si particles are uniformly covered by pyrolytic carbon layer with several nanometers, which demonstrates the well deposition of PANI on the surface of Si particles. After the composite was assembled with graphene, the clear distribution of C and Si elementals, as shown Figure 3d−f, further confirms the encapsulation of Si in graphene sheets.

To further disclose electrochemical properties, the fabricated composites are characterized using half cells with a Li foil as the counter electrode. Figure 4 shows the typical cyclic voltammetry (CV) curves of the Si@C/RGO composite of first, third and fifth cycles in the potential window of 0.01−1.5 V (vs Li/Li^+). In the cathodic part of first cycle, a peak at 1.16 V is ascribed to the formation of SEI, which disappears in the following cycles and, hence, results in the initial irreversible capacity.[8,23] The sharp peak located below 0.1 V represents the alloy reaction of lithium ion and crystallized Si. In the subsequent cycles, the cathodic peak at 0.1 V is replaced by the peak at 0.17 V, because of the amorphization process of crystalline Si during the initial lithiation process.[24] The anodic part displays predominant peak at 0.52 V of first, third, and fifth cycles, which is attributed to the dealloying reaction of Li−Si alloy and the formation of amorphous Si.[25,26]

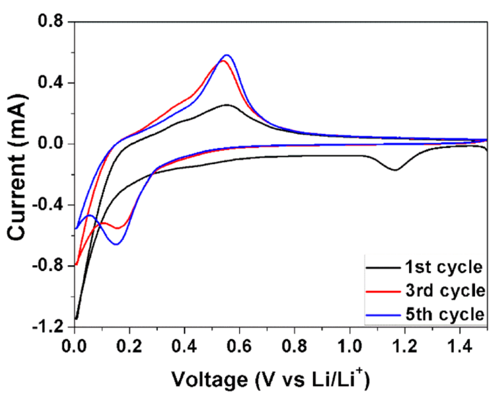

Figure 4. Cyclic voltammetry curves of the Si@C/RGO electrode of first, third, and fifth cycles.

Figure 5a exhibits the first discharge−charge voltage profiles of three different electrodes with a current density of 0.3 A g^{-1}, between voltage limits of 0.01−1.5 V (vs Li/Li^+). Si particles, Si@C and Si@C/RGO electrodes deliver first discharge capacity of 3030, 2798, and 2011 mAh g^{-1}, respectively. Notably, the discharge potential plateaus of these three electrodes are overlapped at near 0.1 V, which agrees well with the lithiation process of crystallized Si.[9,27] Therefore, it is reasonable to speculate that the discharge capacity of the composites are mainly provided by Si, and the carbon or graphene content result in distinct reduction of the discharge capacity. The first charge capacity of Si nanoparticles, Si@C, and Si@C/RGO electrodes are 1703, 2023, and 1630 mAh g^{-1}. The corresponding irreversible capacity, caused by inevitable formation of SEI and side reactions between lithium ion and electrolyte,[28] is obviously reduced after assembled with carbon and graphene sheets gradually. Meanwhile, the initial Coulombic efficiency increases from 56.2% of Si to 72.3% of Si@C remarkably, and further up to 81.1% of Si@C/RGO electrodes, implying that the carbon layer and graphene overcoat are efficient to stabilize the SEI membrane and suppress the side reaction.[13,29]

Figure 5b exhibits the discharge−charge curves of Si@C/RGO electrode from fifth to 200th cycles at a current density of 0.9 A g^{-1}. The first discharge potential plateau of Si@C/RGO shown in Figure 5a is replaced by a group of sloping curves, mainly because of the amorphization process of crystallized Si nanoparticles during the first cycle, which is consistent with the CV results.[30,31] From fifth to 200th cycles, the discharge curves are superimposed closely, manifesting the good reversible electrochemical reaction between lithium ion and Si@C/RGO electrode.

Furthermore, the cycling behavior of Si nanoparticles, Si@C, and Si@C/RGO composites is evaluated by galvanostatic discharge−charge measurements, as shown in Figure 5c. Clearly, the cycling performance of Si@C/RGO composite is superior to that of bare Si nanoparticles and Si@C composite. Although the highest initial discharge capacity, the bare Si nanoparticles display a rapid capacity decline from over 3000 to less than 50 mAh g^{-1} at 0.3 A g^{-1} after 50 cycles, because of inherent disadvantageous properties of Si anode such as huge volume change. After coated with carbon, the cyclability of Si@C composite has a slight improvement and retains at ∼495 mAh g^{-1} at 0.3 A g^{-1} after 50 cycles, which is mainly due to the advantageous carbon layer with aforementioned properties. As for Si@C/RGO electrode, the cyclability and capacity retention has made a distinguished progress. From sixth to 20th cycles, the specific capacity of Si@C/RGO retains 510 mAh g^{-1} at 3 A g^{-1}. As the current density decreased to 0.9 A g^{-1}, the reversible capacity keeps stable at 1121 mAh g^{-1} even over 230 cycles, indicating good cycling ability. Meanwhile, the corresponding Coulombic efficiency of Si@C/RGO composite reaches to over 98% after several cycles with relatively high initial efficiency of 81.1%, which is meaningful for practical application.

In addition, Figure 5d reveals the rate capability of the Si@C/RGO electrode at different current densities ranging from 0.5 to 20 A g^{-1}. The electrode delivers the average discharge capacities of 1226, 948, 726, 588, 548, 492, 388, 274, and 232 mA h g^{-1} at current densities of 0.5, 1, 2, 3.0, 4, 6, 10, 15, and 20 A g^{-1}, respectively. After the ultrahigh rate charge/discharge cycling of 20 A g^{-1}, the specific capacity as high as 1148 mA h g^{-1} can be restored when the current density is returned back to 0.5A g^{-1}, suggesting outstanding rate performance.

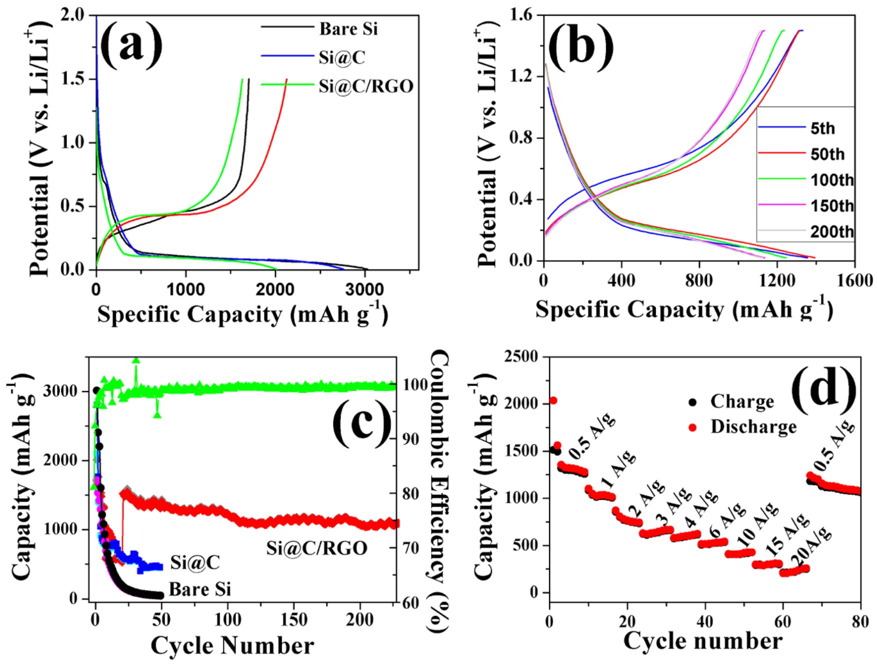

Figure 5. (a) Initial discharge−charge voltage profiles of bare Si, Si@C, and Si@C/RGO. (b) Discharge−charge voltage profiles for Si@C/RGO of fifth, 50th, 100th, 150th, and 200th cycles. (c) Cycling behavior of the Si, Si@C, and Si@C/RGO electrodes. (d) Rate performance of the as-prepared Si@C/RGO composite with increasing current densities from 0.5 to 20 A g^{-1}.

Figure 6 shows Nyquist plots of Si, Si@C, and Si@C/RGO electrodes. The charge-transfer impedance in the electrode/electrolyte interface can be estimated by the diameter of the semicircle in the high-frequency range.[17] As can be seen, Si electrode shows the highest surface layer resistance. Remarkably, the layer resistance of Si@C electrode is greatly reduced. And the Si@C/RGO electrode presents the smallest surface layer resistance among three electrodes. It is believed that the carbon layer is helpful for improving the electron/ion transfer during electrochemical reaction and the wrapped RGO would further enhance the conductivity.

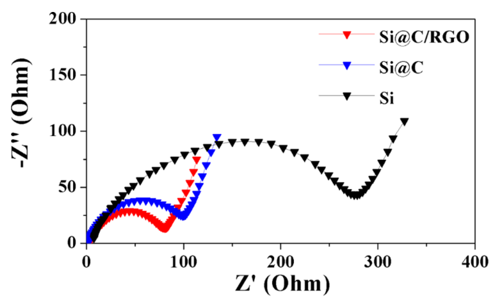

Figure 6. Nyquist plots of the Si, Si@C, and Si@C/RGO electrodes.

Compared with bare Si and Si@C, the Si@C/RGO composite exhibits the improved initial Coulombic efficiency, high reversible capacity, good cyclability, and rate capability. The enhanced performance of Si@C/RGO may be attributed to the following aspects: First, carbon layer, pyrolyzed from polymerized PANI, serves as contact inhibitor to facilitate the formation of stable SEI film and suppress the aggregation among Si nanoparticles during repeated lithium ion insertion/extraction process, which mainly results in improved initial Coulombic efficiency. Second, the RGO sheets are robust and flexible to accommodate the repeated volume changes of the inner Si nanoparticles during cycling and, thus, effectively maintain the structural integrity, which leads to high reversible retention and enhanced cycling stability. Moreover, carbon layer, interconnected with wrapped RGO overcoat, forms a continuous conductive carbonaceous network allowing for fast electron/ion transport during cycling at relatively high current density.

■ CONCLUSION

We have developed a novel method to fabricate Si@C/RGO composite with coated carbon and graphene on Si particles, which can effectively overcome the intrinsic drawbacks of Si anode such as huge volume change and low conductivity. During this synthetic procedure, PANI is introduced as glue to promote the combination of Si nanoparticles with graphene through electrostatic attraction and subsequently thermally decomposed as carbon layer coated on Si surface, which endow the composites with dual protection of carbon and graphene. In this unique architecture, carbon layer and graphene overcoat synergistically provide a conductive and protective matrix to maintain the structural and electrical integrity of the electrode, while Si nanoparticles serve as the lithium-ion storage material with high specific capacity. As a result, Si@C/RGO electrode exhibits enhanced electrochemical performance with high reversible specific capacity of 1121 mAh g^{-1} at 0.9 A g^{-1} over 230 cycles, and improved initial Coulombic efficiency of 81.1%. This method opens up a novel coating strategy for enhanced Si-based anode materials and can be extended to other fascinating anode and cathode materials for next generation of lithium-ion battery.

■ ASSOCIATED CONTENT

Ⓢ Supporting Information

Digital photos of Si, GO, and Si@PANI suspension, GO synthetic procedure, and Raman spectrum of GO. This material is available free of charge via the Internet at http://pubs.acs.org.

AUTHOR INFORMATION

Corresponding Authors

*E-mail: ytqian@ustc.edu.cn. (Y.Q.)
*E-mail: ychzhu@ustc.edu.cn. (Y.Z.)

Funding

This work is supported by the 973 Project of China (No. 2011CB935901) and the National Natural Science Fund of China (Nos. 91022033, 21201158).

Notes

The authors declare no competing financial interest.

ACKNOWLEDGMENTS

We thank the 973 Project of China (No. 2011CB935901), and the National Natural Science Fund of China (Nos. 91022033, 21201158).

REFERENCES

(1) Choi, J. Y.; Lee, D. J.; Lee, Y. M.; Lee, Y. G.; Kim, K. M.; Park, J. K.; Cho, K. Y. Silicon Nanofibrils on a Flexible Current Collector for Bendable Lithium-Ion Battery Anodes. *Adv. Funct. Mater.* **2013**, *23*, 2108−2114.

(2) Zhou, X. S.; Wan, L. J.; Guo, Y. G. Electrospun Silicon Nanoparticle/Porous Carbon Hybrid Nanofibers for Lithium-Ion Batteries. *Small* **2013**, *9*, 2684−2688.

(3) Wang, Y. L.; Wang, T. Y.; Da, P. M.; Xu, M.; Wu, H.; Zheng, G. F. Silicon Nanowires for Biosensing, Energy Storage, and Conversion. *Adv. Mater.* **2013**, *25*, 5177−5195.

(4) Kim, H.; Han, B.; Choo, J.; Cho, J. Three-Dimensional Porous Silicon Particles for Use in High-Performance LithiumSecondary Batteries. Angew. *Chem. Int. Ed.* **2008**, *47*, 10151−10154.

(5) Li, B. J.; Cao, H. Q.; Shao, J.; Qu, M. Z. Enhanced Anode Performances of the Fe3O4−Carbon−rGO Three Dimensional Composite in Lithium-ion Batteries. *Chem. Commun.* **2011**, *47*, 10374−10376.

(6) Wang, B.; Li, X.; Zhang, X.; Luo, B.; Jin, M.; Liang, M.; Dayeh, S. A.; Picraux, S. T.; Zhi, L. J. Adaptable Silicon/Carbon Nanocables Sandwiched between Reduced Graphene Oxide Sheets as Lithium Ion Battery Anodes. *ACS Nano* **2013**, *7*, 1437−1445.

(7) Xue, D. J.; Xin, S.; Yan, Y.; Jiang, K. C.; Yin, Y. X.; Guo, Y. G.; Wan, L. J. Improving the Electrode Performance of Ge through Ge@C Core−Shell Nanoparticles and Graphene Networks. *J. Am. Chem. Soc.* **2012**, *134*, 2512−2515.

(8) Ye, Y. S.; Xie, X. L.; Rick, J.; Chang, F.; Hwang, B. Improved Anode Materials for Lithium-Ion Batteries Comprise Non-covalently Bonded Graphene and Silicon Nanoparticles. *J. Power Sources* **2014**, *247*, 991−998.

(9) Zhu, Y. H.; Liu, W.; Zhang, X. Y.; He, J. C.; Chen, J. T.; Wang, Y. P.; Cao, T. B. Directing Silicon−Graphene Self-Assembly as a Core/Shell Anode for High-Performance Lithium-Ion Batteries. *Langmuir* **2013**, *29*, 744−749.

(10) Zhou, X. S.; Yin, Y. X.; Wan, L. J.; Guo, Y. G. Self-Assembled Nanocomposite of Silicon Nanoparticles Encapsulated in Graphene through Electrostatic Attraction for Lithium-ion Batteries. *Adv. Energy Mater.* **2012**, *2*, 1086−1090.

(11) Zhang, Z. L.; Wang, Y. H.; Ren, W. F.; Tan, Q. Q.; Chen, Y. F.; Li, H.; Zhong, Z. Y.; Su, F. B. Scalable Synthesis of Interconnected Porous Silicon/Carbon Composites by the Rochow Reaction as High-Performance Anodes of Lithium Ion Batteries. *Angew. Chem., Int. Ed.* **2014**, *53*, 1−6.

(12) Pan, L.; Wang, H.; Tan, L.; Chen, S.; Gao, D.; Li, L. Facile Synthesis of Yolk-shell Structured Si-C Nanocomposites as Anode for Lithium-ion Battery. *Chem. Commun.* **2014**, *50*, 5878−5880.

(13) Li, N.; Jin, S.; Liao, Q.; Cui, H.; Wang, C. X. Encapsulated within Graphene Shell Silicon Nanoparticles Anchored on Vertically Aligned Graphene Trees as Lithium-ion Battery Anodes. *Nano Energy* **2014**, *5*, 105−115.

(14) Bao, Z. H.; Weatherspoon, M. R.; Shian, S.; Cai, Y.; Graham, P. D.; Allan, S. M.; Ahma, G.; Dickerson, M. B.; Church, B. C.; Kang, Z. T.; Abernathy, H. W.; Summers, C. J.; Liu, M. L.; Sandhage, K. H. Chemical Reduction of Three-dimensional Silica Micro-assemblies into Microporous Silicon Replicas. *Nature* **2007**, *446*, 172−175.

(15) Wu, H.; Yu, G.; Pan, L.; Liu, N.; McDowell, M. T.; Bao, Z. N.; Cui, Y. Stable Li-ion Battery Anodes by in-situ Polymerization of Conducting Hydrogel to Conformally Coat Silicon Nanoparticles. *Nat. Commun.* **2013**, *4*, 1943.

(16) Lee, J. K.; Smith, K. B.; Hayner, C. M.; Kung, H. H. Silicon Nanoparticles−Graphene Paper Composites for Li-ion Battery Anodes. *Chem. Commun.* **2010**, *46*, 2025−2027.

(17) Hu, Y. S.; Demir-Cakan, R.; Titirici, M. M.; Antonietti, M.; Maier, J. Superior Storage Performance of a Si@SiO_x/C Nanocomposite as Anode Material for Lithium-Ion Batteries. *Angew. Chem., Int. Ed.* **2008**, *47*, 1645−1649.

(18) Wang, J. Z.; Zhong, C.; Chou, S. L.; Liu, H. K. Flexible Free-standing Graphene-Silicon Composite Film for Lithium-ion Batteries. *Electrochem. Commun.* **2010**, *12*, 1467−1470.

(19) Ju, Z. C.; Wang, T. T.; Wang, L. C.; Xing, Z.; Xu, L. Q.; Qian, Y. T. A Simple Pyrolysis Route to Synthesize Leaf-like Carbon Sheets. *Carbon* **2010**, *48*, 3420−3426.

(20) Pielichowski, K. Kinetic Analysis of the Thermal Decomposition of Polyaniline. *Solid State Ionics* **1997**, *104*, 123−132.

(21) Murugan, A. V.; Muraliganth, T.; Manthiram, A. Rapid, Facile Microwave-Solvothermal Synthesis of Graphene Nanosheets and Their Polyaniline Nanocomposites for Energy Storage. *Chem. Mater.* **2009**, *21*, 5004−5006.

(22) Cong, H. P.; Ren, X. C.; Wang, P.; Yu, S. H. Flexible Graphene−Polyaniline Composite Paper for High-Performance Supercapacitor. *Energy Environ. Sci.* **2013**, *6*, 1185−1191.

(23) Lee, S. E.; Kim, H. J.; Park, J. H.; Choi, D. Highly Robust Silicon Nanowire/Graphene Core−Shell Electrodes without Polymeric Binders. *Nanoscale* **2013**, *5*, 8986−8991.

(24) Lin, F.; Nordlund, D.; Weng, T.; Zhu, Y.; Ban, C. L.; Richards, R. M.; Xin, L. Phase Evolution for Conversion Reaction Electrodes in Lithium-ion Batteries. *Nat. Commun.* **2014**, *5*, 3358.

(25) Xia, D.; Xue, Q. Z.; Xie, J.; Chen, H. J.; Lv, C. Silicon/Graphene Core/Shell Nanowires Produced by Self-scrolling. *Comput. Mater. Sci.* **2010**, *49*, 588−592.

(26) Gauthier, M.; Mazouzi, D.; Reyter, D.; Lestriez, B.; Moreau, P.; Guyomard, D. A Low-cost and High Performance Ball-milled Si-based Negative Electrode for High-energy Li-ion Batteries. *Energy Environ. Sci.* **2013**, *6*, 2145−2155.

(27) Xiang, H. F.; Zhang, K.; Lee, J. Y.; Zou, C. J.; Chen, X. D.; Wu, J. S. Graphene/Nanosized Silicon Composites for Lithium Battery Anodes with Improved Cycling Stability. *Carbon* **2011**, *49*, 1787−1796.

(28) Lu, M.; Tian, Y. Y.; Zheng, X. D.; Gao, J.; Huang, B. Preparation, Characterization and Electrochemical Performance of Silicon Coated Natural Graphite as Anode for Lithium Ion Batteries. *Int. J. Electrochem. Sci.* **2012**, *7*, 6180−6190.

(29) Guo, J. C.; Wang, C. S. A Polymer Scaffold Binder Structure for High Capacity Silicon Anode of Lithium-ion Battery. *Chem. Commun.* **2010**, *46*, 1428−1430.

(30) Wang, C. D.; Chui, Y. S.; Ma, R. G.; Wong, T. L.; Ren, J. G.; Wu, Q. H.; Chen, X. F.; Zhang, W. J. A Three-dimensional Graphene Scaffold Supported Thin Film Silicon Anode for Lithium-ion Batteries. *J. Mater. Chem. A* **2013**, *1*, 10092−10098.

(31) Yang, Y.; Ren, J. G.; Wang, X.; Chui, Y. S.; Wu, Q. H.; Chen, X. F.; Zhang, W. J. Graphene Encapsulated and SiC Reinforced Silicon Nanowires As an Anode Material for Lithium ion Batteries. *Nanoscale* **2013**, *5*, 8689−8694.